

Gas Phase Polyalanine: Assessment of $i \rightarrow i + 3$ and $i \rightarrow i + 4$ Helical Turns in $[\text{Ala}_n + 4\text{H}]^{4+}$ ($n = 29\text{--}49$) Ion

Anne E. Counterman[†] and David E. Clemmer*

Department of Chemistry, Indiana University, Bloomington, Indiana 47405

Received: June 6, 2002; In Final Form: September 4, 2002

The structures of a series of quadruply protonated polyalanine peptides ($[\text{Ala}_n + 4\text{H}]^{4+}$, $n = 29\text{--}49$) have been examined in the gas phase using high-pressure drift tube/mass spectrometry and molecular modeling techniques. The results indicate that $[\text{Ala}_n + 4\text{H}]^{4+}$ ions favor stretched helices; $i \rightarrow i + 3$ and $i \rightarrow i + 4$ hydrogen-bonding interactions are significant in stabilizing the extended structures. Experiment and theory indicate that the fraction of $i \rightarrow i + 4$ interactions increases with increasing polymer length. It appears that $i \rightarrow i + 3$ interactions stabilize smaller polymers, where repulsive Coulombic interactions are greater. For $[\text{Ala}_{36} + 4\text{H}]^{4+}$, $\sim 35\%$ of hydrogen-bonding interactions are associated with $i \rightarrow i + 3$ contacts, while $\sim 65\%$ correspond to $i \rightarrow i + 4$ associations. In the larger $[\text{Ala}_{48} + 4\text{H}]^{4+}$ polymer, $\sim 85\%$ of residues are involved in $i \rightarrow i + 4$ hydrogen-bonding interactions.

Introduction

Since Pauling's original prediction of α -helices (networks of $i \rightarrow i + 4$ hydrogen bonds along a polypeptide chain, where i corresponds to each residue along the polymer length),¹ a significant effort has been made to understand factors that influence helix formation. Figure 1 illustrates three types of helices that are found in the architecture of proteins: a 3_{10} -helix, characterized by $i \rightarrow i + 3$ interactions; an α -helix, having $i \rightarrow i + 4$ hydrogen bonds; and a π -helix, with $i \rightarrow i + 5$ interactions. Relative to the 3_{10} - and α -helices, the π -helix is less common, typically established only for short regions of sequence. For a given polymer length, the 3_{10} -helix allows one more hydrogen bond to be formed than an α -helical configuration. However, $i \rightarrow i + 3$ hydrogen bonds are strained relative to $i \rightarrow i + 4$ bonds.² Studies of alanine-rich peptides in solution by NMR suggest that $i \rightarrow i + 4$ hydrogen-bonding networks unfold through structures that are stabilized by networks of $i \rightarrow i + 3$ hydrogen bonds— 3_{10} -helical intermediates.³ Theory also supports this mechanism.⁴ Although the relationship of α - and 3_{10} -helices in folding is emerging, the intrinsic properties associated with the polypeptide chain are not resolved.^{5–10} Molecular dynamics (MD) studies of Ala_n ($n = 8, 10, \text{ and } 11$) in vacuo indicate that α -helical forms should be more stable than 3_{10} -helices by at least ~ 1 kcal mol⁻¹ residue⁻¹,^{7,8,10} while higher level quantum chemical calculations suggest that the 3_{10} -helix should be more stable by 6.5 and 4.9 kcal mol⁻¹ for 6 and 10 residue polymers.¹¹

Here, we report combined drift tube/mass spectrometry (MS) and molecular modeling studies of $[\text{Ala}_n + 4\text{H}]^{4+}$ ($n = 29\text{--}49$) ions. These results indicate that in the gas phase, $i \rightarrow i + 3$ and $i \rightarrow i + 4$ hydrogen-bonding interactions are important in stabilizing extended structures for polymers containing 29 to ~ 49 residues. For small sizes such as $n = 32\text{--}36$, $\sim 30\text{--}40\%$ of alanine residues participate in $i \rightarrow i + 3$ hydrogen bonding; for larger polymers (e.g., $n = 48$), conformers are mostly α -helical ($\sim 85\%$ of alanine residues participate in $i \rightarrow$

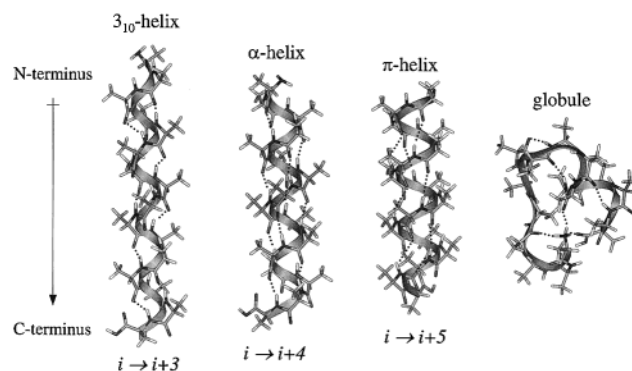


Figure 1. Schematic of 3_{10} -, α -, and π -helical conformations and a representative globular conformer obtained for $[\text{Ala}_{16} + \text{H}]^+$ by Samuelson and Martyna (ref 4). Dotted lines are used to represent hydrogen bonds.

$i + 4$ hydrogen bonding). This study is related to our recent report of several conformer families of gas phase polyalanine peptides ($[\text{Ala}_n + z\text{H}]^{z+}$; $n = 5\text{--}49$, $z = 1\text{--}4$), including extended α -helices and a family of folded states attributed to helix coils.¹²

Assessment of peptide structure in the gas phase is possible because of key advances in biological ion sources^{13,14} for MS and the development of structural techniques, including several ion molecule reactivity probes, such as hydrogen–deuterium exchange,¹⁵ small molecule adduction,^{16,17} and gas phase basicity measurements;^{15d,18} determination of collision- and photon-induced fragmentation patterns;¹⁹ kinetic energy release distributions;²⁰ microscopy studies of surfaces exposed to high-energy ion impacts;²¹ and measurements of collision cross-sections by ion scattering²² and ion mobility^{23–25} techniques. It is noteworthy that in some cases, gas phase ions appear to retain some elements of structure found in solution;^{26–29} in other cases, it appears that it is possible to stabilize structures in the gas phase that have not been observed in solution.^{25b}

The current studies are also related to a number of studies of helix stability in gas phase alanine-based peptides.^{18g,20c,30–32} Despite the high helix propensity of alanine in solution,³³ $[\text{Ala}_n$

[†] Current address: Department of Chemistry, Pennsylvania State University, University Park, PA 16802.

+ H]⁺ ($n \approx 10$ – 20) ions produced by electrospray ionization favor roughly spherical, globular states, in which the protonated N-terminal amino group is solvated by electronegative backbone carbonyl groups.^{30,31} This type of structure is also illustrated in Figure 1. Several other studies of peptide ion conformation report evidence for helices.^{18g,20c} Hudgins, Ratner, and Jarrold found that by adding a single basic lysine residue as the C-terminal residue (i.e., Ala_{*n*}Lys sequences), $i \rightarrow i + 4$ helices were stabilized for singly charged ions.³¹ The C-terminal location of a proton allows favorable interaction with the helix macrodipole. Other studies have examined the stability of alanine helices with respect to number and position of substituted glycine residues (which are helix destabilizing).³² For example, recent gas phase studies show evidence that [Ac-(AGG)₅K + H]⁺ peptides unfold through an untwisted helical state that involves some $i \rightarrow i + 6$ hydrogen bonding.³⁴

Experimental Section

Ion Mobility/Time-of-Flight Measurements. Ion mobility/time-of-flight methods for analyzing peptide mixtures have been described previously,^{35–37} only a brief description is given here. Solutions of polyalanine (Sigma, nominal 1000–5000 mol wt range; 5.6×10^{-5} to 2.8×10^{-4} M in a 49:49:2 water:acetonitrile:acetic acid mixture) were electrosprayed¹³ at atmospheric pressure into a differentially pumped desolvation region, and ions were introduced into the drift region through an ion channel.³⁸ Pulses (300 μ s in duration) of ions were gated into the drift region, where the ions drift ~ 58.23 cm through ~ 160 Torr of He buffer gas under the influence of a uniform 137.4 V cm⁻¹ field. Ions exiting the drift region were focused into the source region of an orthogonal reflectron time-of-flight mass spectrometer. Here, high-voltage pulses synchronous with the initial drift gate pulses were used to initiate m/z measurements. Because flight times in the mass spectrometer are much shorter than drift times in the drift tube, hundreds of flight-time distributions can be recorded for each pulse of ions that is gated into the drift tube. Data were acquired using a nested acquisition system that was developed in-house and described previously.³⁹

Experimental Collision Cross-Sections and Asphericities. The measured arrival times include the time required for ions to travel through drift gas as well as other regions of the instrument. To determine mobilities and cross-sections, it is necessary to correct the arrival times by the time ions spend in other regions of the instrument. These corrections are small (80–140 μ s) relative to the 10–20 ms drift times. The drift velocity (v_D) of an ion is related to the mobility (K) and electric field strength (E) by $v_D = KE$. Measurements are typically derived from the corrected arrival times and reported as reduced mobilities (K_0) or collision cross-sections (Ω), given by the following relations:³⁷

$$K_0 = (L/t_D E) (P/760) (273.2/T) \quad (1)$$

and

$$\Omega = \frac{(18\pi)^{1/2}}{16} \frac{ze}{(k_B T)^{1/2}} \left[\frac{1}{m_I} + \frac{1}{m_B} \right]^{1/2} \frac{t_D E}{L} \frac{760}{P} \frac{T}{273.2} \frac{1}{N} \quad (2)$$

where t_D is the drift time (determined from the maximum of each peak); T and P are the temperature and pressure of the buffer gas, respectively; L is the drift tube length; ze is the ion's charge; N is the neutral number density; k_B is Boltzmann's constant; and m_I and m_B are the masses of the ion and buffer gas, respectively. All of the parameters, E , L , P , T , and t_D , can

be precisely measured. The reproducibility of measured cross-sections is excellent; the percent relative uncertainty of any two measurements is typically less than $\pm 1.0\%$. Measurements were performed at low E/N such that mobilities are independent of the applied drift field, and drift velocities are small compared with the thermal velocity of the buffer gas. Under these conditions, ions are not expected to align in the drift tube and we assume that collision cross-sections correspond to an average of all possible orientations.

To emphasize structural differences between different conformer families and remove the molecular weight dependence of cross-section, we previously defined an effective asphericity scale.¹² Effective asphericities for different peptide lengths (n) are determined from experimental or calculated cross sections (Ω) using

$$\Omega_{\text{asp}} = (\Omega - \Omega_{\text{sphere}}) / (\Omega_{\text{linear}} - \Omega_{\text{sphere}}) \quad (3)$$

where Ω_{sphere} and Ω_{linear} are cross-sections calculated from fits to globular and extended linear geometries.⁴⁰ The asphericity of an ion provides insight about how closely the geometry resembles a tightly packed spherical conformation. A tightly folded compact globular family is defined to have a Ω_{asp} value of 0.0, and a completely extended linear string geometry is assigned $\Omega_{\text{asp}} \equiv 1.0$.

Information about the number of different conformations that are present within a resolved peak can be obtained by comparing experimental peak shapes to the peak shape that is calculated from the transport equation:⁴¹

$$\Phi(t) = \int \frac{C}{(Dt)^{1/2}} [v_D + (L/t)] \left[1 - \exp\left(\frac{-r_o^2}{4Dt}\right) \right] \times \exp\left(\frac{-(L - v_D t)^2}{4Dt}\right) P(t_p) dt_p \quad (4)$$

Here, $\Phi(t)$ is the intensity of ions passing through the exit aperture as a function of time, r_o is the entrance aperture radius, v_D is the measured drift velocity, C is a constant, $P(t_p) dt_p$ is the distribution function for the pulse of ions entering the drift tube, and D is the diffusion constant.⁴² When the experimental arrival time distribution is broader than the calculated distribution, at least two conformer types having similar collision cross-sections must be present or conformers must be interconverting over the time scale of the experiment. In cases where the experimental and calculated distributions are essentially identical, the agreement suggests that a single conformer type may be present. However, we cannot rule out the possibility that two conformers have identical cross-sections.

Molecular Modeling. The [Ala_{*n*} + 3H]³⁺ ($n = 18, 24, 27, 30,$ and 36) and [Ala_{*n*} + 4H]⁴⁺ ($n = 32, 36, 44,$ and 48) ions were modeled with the InsightII molecular modeling software using the extensible systematic force field (ESFF)⁴³ as described previously.¹² In most cases, α -helical starting conformations were used (i.e., all torsion angles were fixed to $\phi = -57^\circ$ and $\psi = -47^\circ$). MD simulations were performed at 300 K for 0.25 ns (and up to 1.0 ns), with 1 fs time step. A number of simulations were also run using 3_{10} -helical and extended starting structures.

As in simulations of [Ala_{*n*} + 3H]³⁺ ions, consideration of many different initial charge site configurations is imperative. For the [Ala₃₆ + 4H]⁴⁺ ion, there are 58 905 [$36!/(4! \times (36-4)!)$] possible charge assignments, assuming that protonation sites are fixed at the N terminus or amide groups on the polymer backbone.⁴⁴ To sample many different conformations, at least

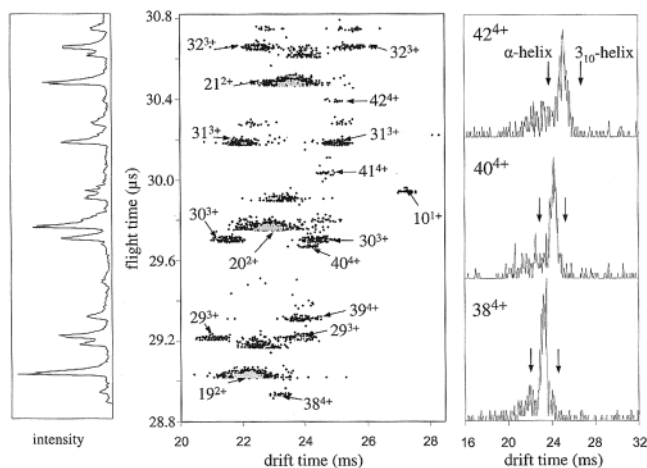


Figure 2. Plot of drift and flight times for a small region (corresponding to m/z 675–825) of a polyalanine mixture. The data have been normalized to a buffer gas pressure of 163.5 Torr and electric field strength of 137.4 V cm^{-1} . All peaks assignable to polyalanine peptides are labeled using the notation n^{z+} (where n is the number of alanines in the polymer chain and z is the protonation state). Unlabeled peaks correspond to unassignable features that are observed at $m = 14$ units above each major peak. The mass spectrum shown on the left was obtained by summing intensity information across all drift times for each flight time. On the right are drift time distributions for $[\text{Ala}_{38} + 4\text{H}]^{4+}$, $[\text{Ala}_{40} + 4\text{H}]^{4+}$, and $[\text{Ala}_{42} + 4\text{H}]^{4+}$ obtained by taking slices through the two-dimensional data set. Arrows indicate the drift time positions expected for ideal α -helical (left) and 3_{10} -helical (right) geometries.

10 widely different charge site assignments were chosen for each polymer size modeled.

Calculation of Cross-Section for Trial Conformers. We have calculated collision cross-sections for all trial conformers as described previously.¹² These values were calculated using the exact hard spheres scattering method (EHSS)⁴⁵ that has been normalized to values expected from a more rigorous trajectory calculation⁴⁶ based on a comparison of values obtained by the two methods for Ala_n α -helices from $n = 10$ to 50.³¹ Drift times expected for calculated geometries can be derived for comparison with experimental drift time distributions using the experimental conditions, calculated cross-section, and eq 2.

Results and Discussion

Experimental Data and General Trends. Figure 2 shows a two-dimensional plot of nested ion mobility/time-of-flight data recorded for a small region of the distribution of electrosprayed polyalanine ions. The peaks that are observed fall into several types of conformer families: well-separated $[\text{Ala}_n + \text{H}]^+$, $[\text{Ala}_n + 2\text{H}]^{2+}$, and $[\text{Ala}_n + 3\text{H}]^{3+}$ families and a low intensity series of peaks corresponding to $[\text{Ala}_n + 4\text{H}]^{4+}$ ions.⁴⁷ For example, peaks observed at flight times of $28.92 \mu\text{s}$ ($m/z = 681.12$), $29.65 \mu\text{s}$ ($m/z = 716.71$), and $30.02 \mu\text{s}$ ($m/z = 734.37$) are assigned to $[\text{Ala}_{38} + 4\text{H}]^{4+}$ (having calculated $m/z_{\text{calcd}} = 680.95$, isotopic average), $[\text{Ala}_{40} + 4\text{H}]^{4+}$ ($m/z_{\text{calcd}} = 716.50$), and $[\text{Ala}_{41} + 4\text{H}]^{4+}$ ($m/z_{\text{calcd}} = 734.28$), respectively. Two discrete series of peaks are observed for $[\text{Ala}_n + 3\text{H}]^{3+}$ ions: a family having higher mobilities than observed for the $[\text{Ala}_n + 2\text{H}]^{2+}$ family and a family of lower mobility ions. We have previously assigned these families to folded hinged helix coil and extended α -helical structures.¹² For $[\text{Ala}_n + 3\text{H}]^{3+}$ and $[\text{Ala}_n + 4\text{H}]^{4+}$ ions having similar m/z ratios, mobilities for $[\text{Ala}_n + 4\text{H}]^{4+}$ ions are similar to those of the low-mobility $[\text{Ala}_n + 3\text{H}]^{3+}$ ions. For example, the value of $K_0 = 3128 \text{ m}^2 \text{ V}^{-1} \text{ s}^{-1}$ derived

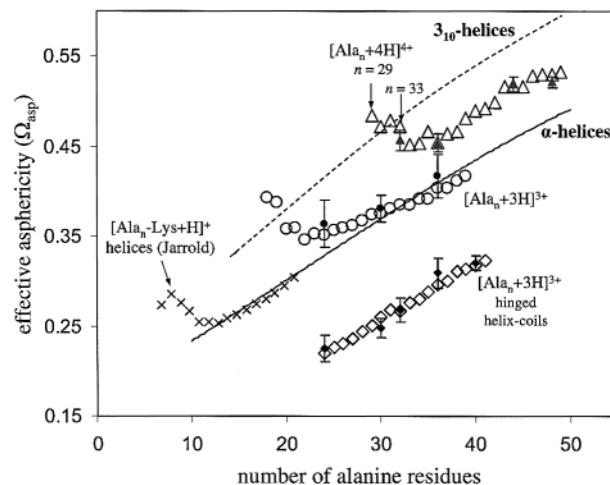


Figure 3. Effective asphericities for $[\text{Ala}_n + 3\text{H}]^{3+}$ ($n = 24\text{--}41$, open diamonds; $n = 18\text{--}39$, open circles) and $[\text{Ala}_n + 4\text{H}]^{4+}$ (open triangles) ions as a function of polymer length. See text for the definition of effective asphericity. Calculated asphericities are shown for model structures obtained from MD simulations for $[\text{Ala}_n + 3\text{H}]^{3+}$ hinged helix coil (solid diamonds; $n = 24, 30, 32, 36,$ and 40) and helical conformers (solid circles; $n = 24, 30,$ and 36) (ref 12) and $[\text{Ala}_n + 4\text{H}]^{4+}$ elongated helical conformers (solid triangles; $n = 32, 36, 44,$ and 48). Uncertainties correspond to one standard deviation of the cross-section calculations for the range of stable states found from molecular modeling. Also shown are asphericities for $[\text{Ala}_n\text{-Lys} + \text{H}]^+$ ions containing 5–19 Ala residues (denoted as \times), derived from relative cross-sections reported previously by Hudgins et al. (ref 31), which have been normalized to account for differences in mass associated with the Lys residue. The solid and dashed lines correspond to calculated values for 10–50 residue ideal α -helical ($\phi = -57^\circ$, $\psi = -47^\circ$) and 3_{10} -helical ($\phi = -49^\circ$, $\psi = -26^\circ$) Ala_n geometries, respectively.

for the $[\text{Ala}_{40} + 4\text{H}]^{4+}$ ion is nearly identical to $K_0 = 3091 \text{ m}^2 \text{ V}^{-1} \text{ s}^{-1}$ for $[\text{Ala}_{30} + 3\text{H}]^{3+}$.

Figure 2 also shows drift time distributions for the $[\text{Ala}_{38} + 4\text{H}]^{4+}$, $[\text{Ala}_{40} + 4\text{H}]^{4+}$, and $[\text{Ala}_{42} + 4\text{H}]^{4+}$ ions ($m/z = 681.0$, 716.5 , and 752.1 , respectively) obtained by integrating the two-dimensional data set over narrow regions of flight time. As indicated in the figure, the drift time distributions for the $[\text{Ala}_n + 4\text{H}]^{4+}$ ions are dominated by narrow peaks having drift times that are intermediate between times expected for ideal α - and 3_{10} -helical model geometries. In each distribution, an additional broad, lower intensity feature is observed at lower drift times than the main peak; drift times of these features are similar to those that we calculated for the ideal α -helical conformer. The full widths at half-maximum (fwhm) of the main $[\text{Ala}_n + 4\text{H}]^{4+}$ peaks are narrow—comparable to those expected for the presence of a single conformer type.⁴¹ The narrow width of the peaks can also be explained by the presence of multiple states that interconvert rapidly as compared with the experimental time scales.

Experimental Asphericities. Figure 3 shows a region of effective asphericities derived from experimental cross-sections for the $[\text{Ala}_n + z\text{H}]^{z+}$ ($n = 18\text{--}49$, $z = 3$ and 4) ions. On this scale, individual $[\text{Ala}_n + \text{H}]^+$ ions, which have previously been shown to be globular and tightly packed,^{4,30,31} have Ω_{asp} values of ~ 0 . The $[\text{Ala}_n + 2\text{H}]^{2+}$ ions are also relatively compact and have Ω_{asp} values that fall below the 0.15 limit shown. Several general trends for the $z = 3$ and 4 polymer families are apparent. First, we note that within a family, asphericities appear to increase with polymer length except at short polymer chain lengths. At these small sizes, the polymers are more aspherical than the average asphericity of the family. One expects that the

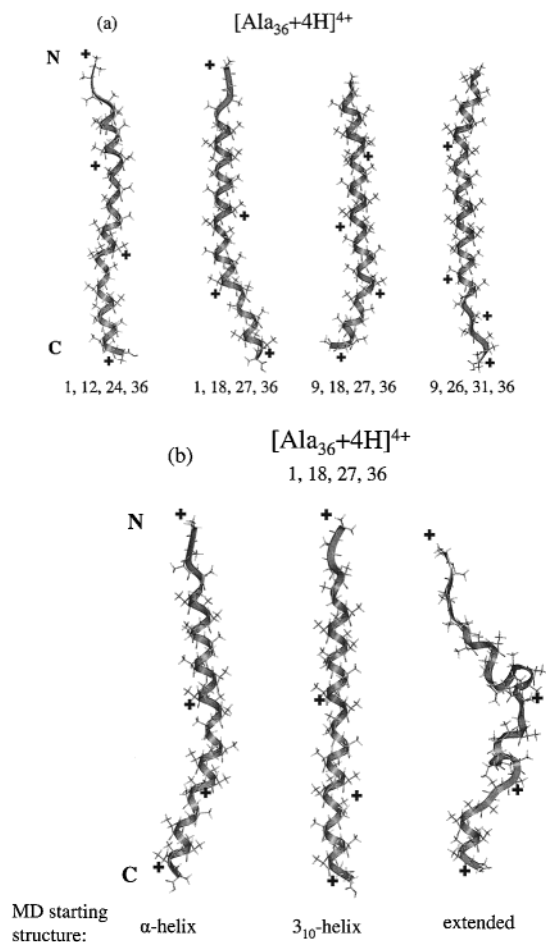


Figure 4. Part (a) shows four typical $[\text{Ala}_{36} + 4\text{H}]^{4+}$ conformers resulting from 300 K MD simulations of the 1, 12, 24, 36 (calculated Ω_{asp} and total energy of 0.449 and $-68.2 \text{ kcal mol}^{-1}$, respectively); 1, 18, 27, 36 (0.467, -78.6); 9, 18, 27, 36 (0.440, -96.2); and 9, 26, 31, 36 (0.449, -95.4) charge assignments in which calculations were initiated from completely α -helical starting structures. Calculated asphericities of these conformers are in agreement with the experimental value of 0.455. Part (b) shows typical $[\text{Ala}_{36} + 4\text{H}]^{4+}$ conformers for the 1, 18, 27, 36 charge assignment obtained from simulations initiated from α -helical (calculated Ω_{asp} and total energy of 0.467 and $-78.6 \text{ kcal mol}^{-1}$, respectively), 3_{10} -helical (0.463, -78.3), and extended linear starting structures (0.467, -28.9). All other conditions of the simulation were identical to those used in part (a). The locations of N and C termini are indicated by "N" and "C", respectively; "+" symbols are used to indicate the charge site positions.

larger coulomb repulsion associated with shorter chain lengths (for high charge states) may force these small polypeptide chains to adopt more extended structures. For the low-mobility $[\text{Ala}_n + 3\text{H}]^{3+}$ family, the asphericity of small polymers decreases from $n = 18$ to $n = 22$. Above this size, the asphericity increases and values of Ω_{asp} become similar to the calculated values for ideal α -helices. As we reported previously¹² (and as shown in Figure 3), molecular modeling simulations lead to structures that are dominated by $i \rightarrow i + 4$ interactions and have calculated Ω_{asp} values that are in good agreement with experiment. Also shown on this plot are asphericity values calculated from the relative cross-sections reported by Hudgins, Ratner, and Jarrold for helical $[\text{Ala}_n\text{Lys} + \text{H}]^+$ peptides.³¹ These values agree with asphericities that we calculated for ideal α -helices but are substantially below Ω_{asp} values calculated for ideal 3_{10} -helices.

Asphericities of the $[\text{Ala}_n + 4\text{H}]^{4+}$ are intermediate between calculated values for α - and 3_{10} -helical forms. This implies that these ions may form stretched α -helices or may be comprised

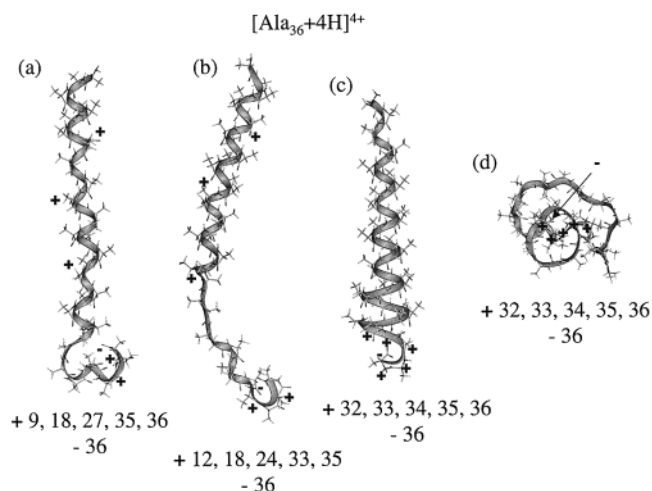


Figure 5. Low energy geometries for salt bridge configurations of $[\text{Ala}_{36} + 4\text{H}]^{4+}$ in which the C terminus is deprotonated at the acidic proton of the carboxylic acid moiety ($i = 36$), and protons are located at 9, 18, 27, 35, 36 (calculated total energy of $-111.4 \text{ kcal mol}^{-1}$); 12, 18, 24, 33, 35 ($-94.2 \text{ kcal mol}^{-1}$); and 32, 33, 34, 35, 36 ($-39.7 \text{ kcal mol}^{-1}$); these conformers were obtained from simulations initiated from ideal α -helical geometries. Part (d) shows a representative low energy geometry for the 32, 33, 34, 35, 36 (and deprotonated at carboxylic acid group on 36) charge configuration (calculated total energy of $-76.9 \text{ kcal mol}^{-1}$) obtained using an extended starting geometry.

of a mixture of 3_{10} - ($i \rightarrow i + 3$) and α -helical ($i \rightarrow i + 4$) hydrogen bonding. It is also possible that the presence of an additional proton in $[\text{Ala}_n + 4\text{H}]^{4+}$ completely destabilizes the helical forms found for the $[\text{Ala}_n + 3\text{H}]^{3+}$ conformers. Molecular modeling simulations were employed to investigate these possibilities.

MD Simulations of $[\text{Ala}_n + 4\text{H}]^{4+}$ Ions. Figure 4 (part a) shows the lowest energy conformers obtained for four different charge configurations of $[\text{Ala}_{36} + 4\text{H}]^{4+}$ (simulations were started from α -helical structures). The overall appearance of the conformers shows a high helical content, similar to results obtained for $[\text{Ala}_{36} + 3\text{H}]^{3+}$ ions.¹² However, because of the increased Coulombic repulsion between charges, initial $i \rightarrow i + 4$ helices unravel slightly. In particular, protonation at the N terminus (e.g., the 1, 12, 24, 36 and 1, 18, 27, 36 conformers shown) destabilizes both $i \rightarrow i + 3$ and $i \rightarrow i + 4$ hydrogen bonding in the N-terminal residues. Throughout the remainder of the polymer chain, a mixture of $i \rightarrow i + 3$ and $i \rightarrow i + 4$ bonding is observed. This result is not unique to simulations started from α -helical structures. Figure 4b compares conformers obtained for the 1, 18, 27, 36 charge assignment using α -helical, 3_{10} -helical, and extended initial structures. The lowest energy conformers obtained from 3_{10} -helical starting structures contain almost identical fractions of $i \rightarrow i + 3$ and $i \rightarrow i + 4$ hydrogen bonds as those conformers obtained from α -helical starting structures. Examination of many replicate simulations started from ideal α - or 3_{10} -helices shows that the exact positions of $i \rightarrow i + 3$ hydrogen bonds vary. Thus, we have not found the lowest energy conformers but appear to have found representative low energy states. Conformers obtained by starting from an extended structure are less ordered and have higher calculated energies; however, by 0.25 ns of simulation, nascent regions of helical conformation usually become apparent. Simulations started from extended structures are limited by the ability of the calculations to sample different conformations over the time scale of the simulation. It should be noted that throughout the simulations, it does not appear that the helix unravels from one of the termini. Instead, the locations of $i \rightarrow i + 3$ perturbation

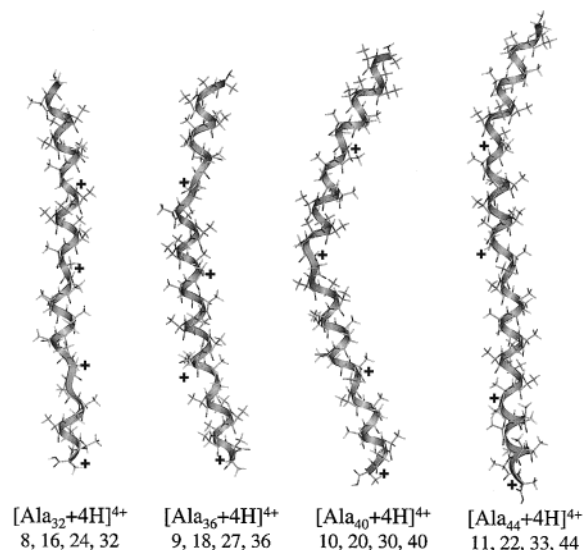


Figure 6. Low energy geometries for $[\text{Ala}_{32} + 4\text{H}]^{4+}$ (8, 16, 24, 32 proton configuration), $[\text{Ala}_{36} + 4\text{H}]^{4+}$ (9, 18, 27, 36), $[\text{Ala}_{40} + 4\text{H}]^{4+}$ (10, 20, 30, 40), and $[\text{Ala}_{44} + 4\text{H}]^{4+}$ (11, 22, 33, 44). All of these $[\text{Ala}_n + 4\text{H}]^{4+}$ conformers have proton configurations of the general form $n/4, n/2, 3n/4, n$. Calculated asphericities for these conformers are in good agreement with experiment (within the uncertainties shown in Figure 3).

or regions of extended structure (no backbone hydrogen bonding) are variable, although there is a higher probability of distortion near a charge site.

Consideration of Salt-Bridged Configurations. Our previous simulations indicated that $[\text{Ala}_{36} + 3\text{H}]^{3+}$ extended helices could not be represented by salt bridge configurations in which the C terminus was deprotonated and four sites along the backbone (including the N terminus) were protonated.¹² Because salt-bridged forms are believed to be more prevalent for higher charge state ions, it is important to test this possibility for the $[\text{Ala}_n + 4\text{H}]^{4+}$ ions. We examined simulations for 10 salt-bridged configurations of $[\text{Ala}_{36} + 4\text{H}]^{4+}$, in which five backbone sites were protonated and the carboxylic acid group on the C terminus was deprotonated. Figure 5 a–c shows representative low-energy conformers obtained from simulations (started from α -helical structures) for three of the charge site assignments. The two lowest energy geometries from the many salt-bridged configurations sampled during the calculations were obtained by placing protons at $i = 9, 18, 27, 35, 36$ (e.g., conformer 5a) or $i = 12, 18, 24, 33, 35$ positions (conformer 5b) and removing the acidic proton on the carboxylic group of the C terminus at $i = 36$. These low-energy conformers are not consistent with experiment; they have calculated cross-sections that are significantly higher (12 and 27%, respectively) than the experimental value. The conformers that showed the closest agreement with the experimental Ω_{asp} value were obtained by placing protons at $i = 32, 33, 34, 35, 36$ (and removing the acidic proton at 36) on an α -helical starting structure; the resulting conformers (part c) have calculated cross-sections slightly lower ($\sim 3\%$) than the experimental value. However, we feel that this structure is unlikely based on comparison of calculated energies; conformer 5c is higher in energy than 5a and 5b by ~ 71.7 and 54.5 kcal mol⁻¹, respectively. Additionally, 5c is higher in energy than other geometries for the 32, 33, 34, 35, 36 (-36) charge configurations that were obtained using completely extended starting structures for simulations (5d). The globlike conformer shown in 5d was obtained under identical simulation conditions (except starting structure) as conformer 5c but is 37.2 kcal mol⁻¹ lower in energy and has a cross-section

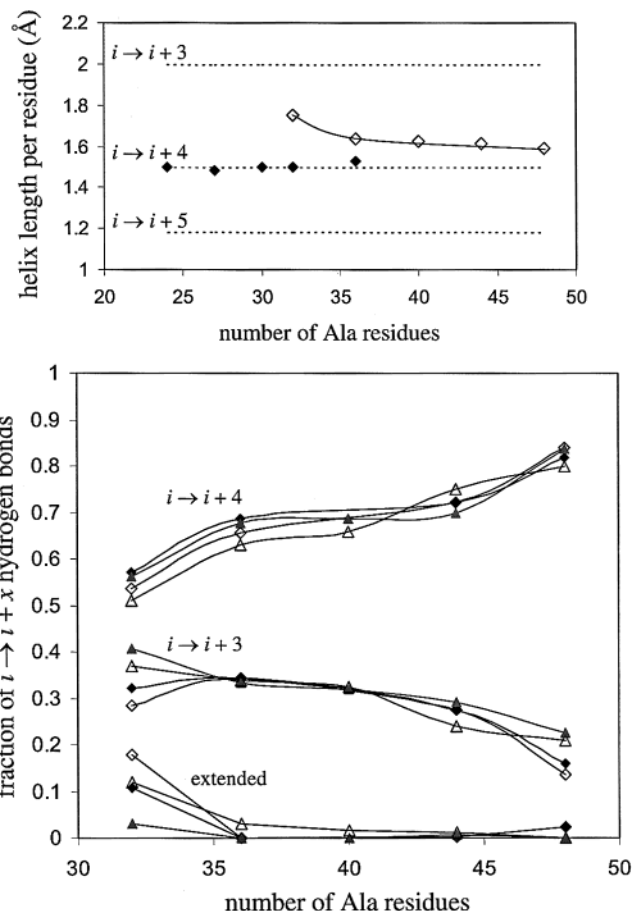


Figure 7. (a) Helix length per residue (\AA) as a function of polymer size for model geometries of $[\text{Ala}_n + 3\text{H}]^{3+}$ and $[\text{Ala}_n + 4\text{H}]^{4+}$ that show good agreement with experimental collision cross-sections. The estimated uncertainty is less than 1.0 \AA over the entire helix length. The solid line is intended as a visual guide. Dashed lines show helix length per residue for ideal $i \rightarrow i + 3$ (3_{10}), $i \rightarrow i + 4$ (α), and $i \rightarrow i + 5$ (π) helices. (b) Fraction of $i \rightarrow i + 3$ and $i \rightarrow i + 4$ hydrogen bonding found in $[\text{Ala}_n + 4\text{H}]^{4+}$ conformations obtained from MD studies of the $n/4, n/2, 3n/4, n$ (solid diamonds); $1, n/2, 3n/4, n$ (open diamonds); $n/3, n/2, 5n/6, n$ (solid triangles); and $n/6, n/3, 2n/3, n$ (open triangles) charge assignments. Solid lines are intended as a visual guide. Values shown are an average for the lowest energy 20 structures for each charge assignment.

that is substantially smaller than experiment. We concluded that zwitterionic forms are not favored for $[\text{Ala}_n + 4\text{H}]^{4+}$ ions.

Fraction of $i \rightarrow i + 3$ and $i \rightarrow i + 4$ Hydrogen Bonding in $[\text{Ala}_n + 4\text{H}]^{4+}$ Ions. We have also examined different charge site configurations for $[\text{Ala}_n + 4\text{H}]^{4+}$ alanine polymers of different lengths. Figure 6 shows representative low-energy conformers obtained for several polymer sizes: $[\text{Ala}_n + 4\text{H}]^{4+}$ $n = 32, 36, 40$, and 44 . The simulations show that the $i \rightarrow i + 4$ and $i \rightarrow i + 3$ content of $[\text{Ala}_n + 4\text{H}]^{4+}$ conformers varies over the size range $n = 32$ – 48 . For small values of n , high Coulombic repulsion between sites on $[\text{Ala}_n + 4\text{H}]^{4+}$ ions causes the system to utilize a higher fraction of $i \rightarrow i + 3$ hydrogen bonding. The $i \rightarrow i + 3$ networks allow the polymer chain to extend; this reduces coulomb repulsion while retaining many hydrogen-bonding interactions. These charge site configurations have calculated asphericities that are in good agreement with experiment; average calculated values are shown in Figure 3.

A measure of the changes in $i \rightarrow i + 4$ and $i \rightarrow i + 3$ helical content that occur with polymer size can be obtained by examining the average length of the helix per residue (measured along the helix axis) and the fraction of $i \rightarrow i + 3$ and $i \rightarrow i +$

4 hydrogen bonding observed for each polymer length. Figure 7 summarizes these results. For $[\text{Ala}_n + 3\text{H}]^{3+}$ helices, the conformer length per residue is essentially constant at a value that is close to the 1.5 Å value of an ideal α -helix. This value is consistent with our previous simulations that showed that conformers for each polymer size are comprised of $\sim 90\%$ $i \rightarrow i + 4$ hydrogen bonding. For $[\text{Ala}_n + 4\text{H}]^{4+}$ helical conformers, the length per residue is intermediate between those calculated for ideal α - and 3_{10} -helices. Values decline from $n = 32$ – 36 , consistent with the relaxation of helical turns into $i \rightarrow i + 4$ configurations with increasing polymer length.

Figure 7 also shows the average fraction of $i \rightarrow i + 3$ and $i \rightarrow i + 4$ hydrogen bonds observed for various sizes of $[\text{Ala}_n + 4\text{H}]^{4+}$ model conformers having general protonation schemes where charges are placed at approximately the $i = n/4, n/2, 3n/4, n; 1, n/2, 3n/4, n; n/3, n/2, 5n/6, n; \text{ and } n/6, n/3, 2n/3, n$. Different polymer sizes ($n = 32, 36, 44, \text{ and } 48$) were simulated multiple times starting from completely α - and 3_{10} -helical structures. The averages of results are in good agreement with experimental asphericity values and have relatively low calculated energies (see, for instance, the conformers shown in Figures 4 and 6). At $n = 32$, the fraction of $i \rightarrow i + 3$ bonding is ~ 25 – 40% ; the number of residues not involved in $i \rightarrow i + 3$ or $i \rightarrow i + 4$ hydrogen bonding is also significant (up to $\sim 18\%$). As n increases, $i \rightarrow i + 4$ hydrogen bonding becomes more favorable. By $n = 48$, $\sim 85\%$ of residues are involved in $i \rightarrow i + 4$ hydrogen-bonding interactions. This is consistent with a model in which $i \rightarrow i + 3$ hydrogen bonding is important in stabilizing helices that are disrupted by Coulombic repulsion. As the polymer length increases, Coulombic repulsion between charge sites also decreases. The system is further stabilized by incorporating $i \rightarrow i + 3$ interactions. This model is similar to results from solution-based studies in which $i \rightarrow i + 3$ hydrogen bonding is implicated as an intermediate in folding an α -helix.⁴⁸

Summary and Conclusions

Ion mobility measurements and molecular modeling techniques have been used to examine conformations of $[\text{Ala}_n + 4\text{H}]^{4+}$ ($n = 29$ – 49) ions. The ion distribution is dominated by a family of extended conformers. Simulations indicate that the $[\text{Ala}_n + 4\text{H}]^{4+}$ ions are stabilized by a significant fraction of $i \rightarrow i + 3$ and $i \rightarrow i + 4$ hydrogen bonds. The fraction of residues involved in $i \rightarrow i + 4$ hydrogen bonding increases with increased polymer length and reaches $\sim 85\%$ for polymer lengths of ~ 48 residues. The increased fraction of $i \rightarrow i + 3$ hydrogen bonding in small $[\text{Ala}_n + 4\text{H}]^{4+}$ conformers helps to relieve repulsive Coulombic interactions while still maintaining many hydrogen bonds.

Acknowledgment. The authors gratefully acknowledge financial support from the National Institutes of Health (Grant No. 1R01GM59145) and the National Science Foundation (CHE-0078737).

References and Notes

- Pauling, L.; Corey, R. B.; Branson, H. R. *Proc. Natl. Acad. Sci. U.S.A.* **1951**, *37*, 205.
- Voet, D.; Voet, J. G. *Biochemistry*, 2nd ed.; Wiley: New York, 1995.
- Millhauser, G. L.; Stenland, C. J.; Hanson, P.; Bolin, K. A.; van de Ven, F. J. M. *J. Mol. Biol.* **1997**, *267*, 963.
- Samuelson, S.; Martyna, G. J. *J. Phys. Chem. B* **1999**, *103*, 1752.
- Vasquez, M.; Nemethy, G.; Scheraga, H. A. *Chem. Rev.* **1994**, *94*, 2183.
- Smythe, M. L.; Huston, S. E.; Marshall, G. R. *J. Am. Chem. Soc.* **1993**, *115*, 11594.
- Tirado-Rives, J.; Maxwell, D. S.; Jorgenson, W. L. *J. Am. Chem. Soc.* **1993**, *115*, 11590–11593.
- Zhang, L.; Hermans, J. *J. Am. Chem. Soc.* **1994**, *116*, 11915–11921.
- Sheinerman, F. B.; Brooks, C. L., III. *J. Am. Chem. Soc.* **1995**, *117*, 10098–10103.
- Wang, Y.; Kuczera, K. *J. Phys. Chem. B* **1997**, *101*, 5205–5213.
- Topol, I. A.; Burt, S. K.; Derety, E.; Tang, T.-H.; Perczel, A.; Rashin, A.; Csizmadia, I. G. *J. Am. Chem. Soc.* **2001**, *123*, 6054.
- Counterman, A. E.; Clemmer, D. E. *J. Am. Chem. Soc.*, **2001**, *123*, 1490.
- Fenn, J. B.; Mann, M.; Meng, C. K.; Wong, S. F.; Whitehouse, C. M. *Science* **1989**, *246*, 64.
- Karas, M.; Hillenkamp, F. *Anal. Chem.* **1988**, *60*, 2299–2301.
- (a) Winger, B. E.; Light-Wahl, K. J.; Rockwood, A. L.; Smith, R. D. *J. Am. Chem. Soc.* **1992**, *114*, 5897. (b) Suckau, D.; Shi, Y.; Beu, S. C.; Senko, M. W.; Quinn, J. P.; Wampler, F. M.; McLafferty, F. W. *Proc. Natl. Acad. Sci. U.S.A.* **1993**, *90*, 790. (c) Wood, T. D.; Chorush, R. A.; Wampler, F. M.; Little, D. P.; O'Connor, P. B.; McLafferty, F. W. *Proc. Natl. Acad. Sci. U.S.A.* **1995**, *92*, 2451. (d) Cassady, C. J.; Carr, S. R. *J. Mass Spectrom.* **1996**, *31*, 247–254.
- Fye, J. L.; Woenckhaus, J.; Jarrold, M. F. *J. Am. Chem. Soc.* **1998**, *120*, 1327.
- (a) McLuckey, S. A.; Goeringer, D. E. *Anal. Chem.* **1995**, *67*, 2493. (b) Stephenson, J. L., Jr.; McLuckey, S. A. *J. Am. Chem. Soc.* **1996**, *118*, 7390. (c) Stephenson, J. L., Jr.; McLuckey, S. A. *Anal. Chem.* **1996**, *68*, 4026. (d) McLuckey, S. A.; Stephenson, J. L., Jr.; Asano, K. G. *Anal. Chem.* **1998**, *70*, 1198. (e) Stephenson, J. L., Jr.; McLuckey, S. A. *J. Am. Chem. Soc. Mass Spectrom.* **1998**, *9*, 585.
- (a) Ogorzalek Loo, R. R.; Smith, R. D. *J. Am. Soc. Mass Spectrom.* **1994**, *5*, 207. (b) Ogorzalek Loo, R. R.; Winger, B. E.; Smith, R. D. *J. Am. Soc. Mass Spectrom.* **1994**, *5*, 1064. (c) Schnier, P. F.; Gross, D. S.; Williams, E. R. *J. Am. Chem. Soc.* **1995**, *117*, 6747. (d) Williams, E. R. *J. Mass Spectrom.* **1996**, *31*, 831. (e) Rodriguez-Cruz, S. E.; Klassen, J. S.; Williams, E. R.; *J. Am. Soc. Mass Spectrom.* **1997**, *8*, 565. (f) Zhang, X.; Cassady, C. J. *J. Am. Soc. Mass Spectrom.* **1996**, *7*, 1211. (g) Sterner, J. L.; Johnston, M. V.; Nicol, G. R.; Ridge, D. P. *J. Am. Soc. Mass Spectrom.* **1999**, *10*, 483.
- (a) Loo, J. A.; Edmonds, C. G.; Smith, R. D. *Science* **1990**, *248*, 201. (b) Wu, Q.; Van Orden, S.; Cheng, X.; Bakhtiar, R.; Smith, R. D. *Anal. Chem.* **1995**, *67*, 2498. (c) Zubarev, R. A.; Kelleher, N. L.; McLafferty, F. W. *J. Am. Chem. Soc.* **1998**, *120*, 3265. (d) Vachet, R. W.; Asam, M. R.; Glish, G. L. *J. Am. Chem. Soc.* **1996**, *118*, 6252.
- (a) Kaltashov, I. A.; Fenselau, C. C. *J. Am. Chem. Soc.* **1995**, *117*, 9906. (b) Adams, J.; Strobel, F.; Reiter, A.; Sullands, M. C. *J. Am. Soc. Mass Spectrom.* **1996**, *7*, 30. (c) Kaltashov, I. A.; Fenselau, C. C. *Proteins* **1997**, *27*, 165.
- (a) Sullivan, P. A.; Axelsson, J.; Altmann, S.; Quist, A. P.; Sunqvist, B. U. R.; Reimann, C. T. *J. Am. Soc. Mass Spectrom.* **1996**, *7*, 329. (b) Reimann, C. T.; Sullivan, P. A.; Axelsson, J.; Quist, A. P.; Altmann, S.; Roepstorff, P.; Velazquez, I.; Tapia, O. *J. Am. Chem. Soc.* **1998**, *120*, 7608.
- (a) Covey, T. R.; Douglas, D. J. *J. Am. Soc. Mass Spectrom.* **1993**, *4*, 616. (b) Cox, K. A.; Julian, R. K.; Cooks, R. G.; Kaiser, R. E. *J. Am. Soc. Mass Spectrom.* **1994**, *5*, 127. (c) Collings, B. A.; Douglas, D. J. *J. Am. Chem. Soc.* **1996**, *118*, 4488. (d) Chen, Y.-L.; Collings, B. A.; Douglas, D. J. *J. Am. Soc. Mass Spectrom.* **1997**, *8*, 681.
- (a) von Helden, G.; Wyttenbach, T.; Bowers, M. T. *Science* **1995**, *267*, 1483. (b) Wyttenbach, T.; von Helden, G.; Bowers, M. T. *J. Am. Chem. Soc.* **1996**, *118*, 8355.
- (a) Clemmer, D. E.; Hudgins, R. R.; Jarrold, M. F. *J. Am. Chem. Soc.* **1995**, *117*, 10141. (b) Shelimov, K. B.; Clemmer, D. E.; Hudgins, R. R.; Jarrold, M. F. *J. Am. Chem. Soc.* **1997**, *119*, 2240. (c) Shelimov, K. B.; Jarrold, M. F. *J. Am. Chem. Soc.* **1997**, *119*, 2987.
- (a) Valentine, S. J.; Clemmer, D. E. *J. Am. Chem. Soc.* **1997**, *119*, 3558. (b) Valentine, S. J.; Anderson, J.; Ellington, A. E.; Clemmer, D. E. *J. Phys. Chem. B* **1997**, *101*, 3891. (c) Valentine, S. J.; Counterman, A. E.; Clemmer, D. E. *J. Am. Soc. Mass Spectrom.* **1997**, *8*, 954.
- Covey, T. R.; Douglas, D. J. *J. Am. Soc. Mass Spectrom.* **1993**, *4*, 616.
- Hudgins, R. R.; Woenckhaus, J.; Jarrold, M. F. *Int. J. Mass Spectrom. Ion Processes* **1997**, *165/166*, 497.
- Suckau, D.; Shi, Y.; Beu, S. C.; Senko, M. W.; Quinn, J. P.; Wampler, F. M.; McLafferty, F. W. *Proc. Natl. Acad. Sci. U.S.A.* **1993**, *90*, 790.
- Li, J.; Taraszka, J. A.; Counterman, A. E.; Clemmer, D. E. *Int. J. Mass Spectrom. Ion Processes* **1999**, *185/186/187*, 37.
- Hudgins, R. R.; Mao, Y.; Ratner, M. A.; Jarrold, M. F. *Biophys. J.* **1999**, *76*, 1591.
- Hudgins, R. R.; Ratner, M. A.; Jarrold, M. F. *J. Am. Chem. Soc.* **1998**, *120*, 12974.
- Kaletka, D. T.; Jarrold, M. F. *J. Phys. Chem. B* **2001**, *105*, 4436.
- See, for example, (a) Chou, P. Y.; Fasman, G. D. *Biochemistry* **1974**, *13*, 211. (b) O'Neil, K. T.; DeGrado, W. F. *Science* **1990**, *250*, 646.

(c) Lyu, P. C.; Liff, M. I.; Marky, L. A.; Kallenbach, N. R. *Science* **1990**, *250*, 669 and references therein.

(34) Kinnear, B. S.; Hartings, M. R.; Jarrold, M. F. *J. Am. Chem. Soc.* **2001**, *123*, 5660.

(35) Hoaglund, C. S.; Valentine, S. J.; Sporleder, C. R.; Reilly, J. P.; Clemmer, D. E. *Anal. Chem.* **1998**, *70*, 2236.

(36) Henderson, S. C.; Valentine, S. J.; Counterman, A. E.; Clemmer, D. E. *Anal. Chem.* **1999**, *71*, 291.

(37) For recent reviews of ion mobility studies of biomolecules, see (a) Clemmer, D. E.; Jarrold, M. F. *J. Mass Spectrom.* **1997**, *32*, 577. (b) Liu, Y.; Valentine, S. J.; Counterman, A. E.; Hoaglund, C. S.; Clemmer, D. E. *Anal. Chem.* **1997**, *69*, 728A. (c) Jarrold, M. F. *Acc. Chem. Res.* **1999**, *32*, 360. (d) Hoaglund Hyzer, C. S.; Counterman, A. E.; Clemmer, D. E. *Chem. Rev.* **1999**, *99*, 3037.

(38) Li, J.; Taraszka, J. A.; Counterman, A. E.; Clemmer, D. E. *Int. J. Mass Spectrom. Ion Processes* **1999**, *185/186/187*, 37.

(39) Hoaglund, C. S.; Valentine, S. J.; Sporleder, C. R.; Reilly, J. P.; Clemmer, D. E. *Anal. Chem.* **1998**, *70*, 2236.

(40) Effective asphericities are calculated using $\Omega_{\text{sphere}} = -9.49 \times 10^{-4} n^3 + -0.213 n^2 + 16.2 n + 38.1$, as determined from a fit to experimental cross sections for globular $[\text{Ala}_n + \text{H}]^+$ ions; and $\Omega_{\text{linear}} = 25.95 n + 27.75$, as determined from a fit to calculated cross-sections (as described in ref 12) for linear structures.

(41) Mason, E. A.; McDaniel, E. W. *Transport Properties of Ions in Gases*; Wiley: New York, 1988.

(42) Under low field conditions, the diffusion constant is related to the measured mobility by the expression $D = Kk_b T / ze$, where K is the mobility, k_b is Boltzmann's constant, and ze is the charge.

(43) *Insight II*; Biosym/MSI: San Diego, CA, 1995.

(44) Consistent with our previous study of $[\text{Ala}_n + 3\text{H}]^{3+}$ ($n = 18-41$) ions (ref 12), we have placed protons only on $-\text{NH}$ groups of the peptide backbone. In general, coulomb repulsion between charge sites is a dominant factor in determining overall conformation in these multiply charged systems. Although we note that theoretical studies of triglycine have suggested that the backbone $-\text{C}=\text{O}$ groups are more basic than backbone $-\text{NH}$ groups (Zhang, K.; Cassady, C. J.; Chung-Phillips, A. *J. Am. Chem. Soc.* **1994**, *116*, 11512), these were not considered as protonation sites due to limitations of the available force fields. Because the electronegativity of carbonyl groups engages them in hydrogen-bonding interactions with the protonation site, it is unlikely that formally placing the proton on the $-\text{NH}$ portion of the backbone will significantly affect the molecular modeling results.

(45) Shvartsburg, A. A.; Jarrold, M. F. *Chem. Phys. Lett.* **1996**, *261*, 86.

(46) Mesleh, M. F.; Hunter, J. M.; Shvartsburg, A. A.; Schatz, G. C.; Jarrold, M. F. *J. Phys. Chem.* **1996**, *100*, 16082.

(47) In some cases, small unassigned peaks that are shifted by $m = 14$ units from expected charge states are also observed [e.g., the peak observed at $29.88 \mu\text{s}$ ($m/z = 728.01$) is 7 u higher than the $[\text{Ala}_{20} + 2\text{H}]^{2+}$ peak observed at $29.74 \mu\text{s}$ ($m/z = 721.00$)]. We have not assigned these ions, and note that they are less intense than related assignable peaks (usually less than 5% as abundant as the $[\text{Ala}_n + z\text{H}]^{z+}$ parents).

(48) See Bolin, K. A.; Millhauser, G. L. *Acc. Chem. Res.* **1999**, *32*, 1027 and references therein.